nature microbiology

ARTICLES

PUBLISHED: 17 OCTOBER 2016 | ARTICLE NUMBER: 16191 | DOI: 10.1038/NMICROBIOL.2016.191

Secreted tryptophanyl-tRNA synthetase as a primary defence system against infection

Young Ha Ahn[1†], Sunyoung Park[2†], Jeong June Choi[2], Bo-Kyung Park[2], Kyung Hee Rhee[3], Eunjoo Kang[4], Soyeon Ahn[5], Chul-Ho Lee[6], Jong Soo Lee[7], Kyung-Soo Inn[8], Mi-La Cho[9], Sung-Hwan Park[10], Kyunghee Park[11,12], Hae Jung Park[11,12], Jae Hyun Lee[11,12], Jung Won Park[11,12], Nam Hoon Kwon[4], Hyunbo Shim[13], Byung Woo Han[3], Pilhan Kim[5], Joo-Youn Lee[1,14], Youngho Jeon[15], Jin Won Huh[16], Mirim Jin[2*] and Sunghoon Kim[1,4*]

The N-terminal truncated form of a protein synthesis enzyme, tryptophanyl-tRNA synthetase (mini-WRS), is secreted as an angiostatic ligand. However, the secretion and function of the full-length WRS (FL-WRS) remain unknown. Here, we report that the FL-WRS, but not mini-WRS, is rapidly secreted upon pathogen infection to prime innate immunity. Blood levels of FL-WRS were increased in sepsis patients, but not in those with sterile inflammation. FL-WRS was secreted from monocytes and directly bound to macrophages via a toll-like receptor 4 (TLR4)–myeloid differentiation factor 2 (MD2) complex to induce phagocytosis and chemokine production. Administration of FL-WRS into *Salmonella typhimurium*-infected mice reduced the levels of bacteria and improved mouse survival, whereas its titration with the specific antibody aggravated the infection. The N-terminal 154-amino-acid eukaryote-specific peptide of WRS was sufficient to recapitulate FL-WRS activity and its interaction mode with TLR4–MD2 is now suggested. Based on these results, secretion of FL-WRS appears to work as a primary defence system against infection, acting before full activation of innate immunity.

The activation of innate immunity is known to be initiated by the complex interaction of exogenous molecules—pathogen-associated molecular patterns (PAMPs)—with pattern recognition receptors (PRRs) such as toll-like receptors (TLRs). However, the existence of human intrinsic factors that can trigger innate immunity remains controversial. Chromatin-associated protein high-mobility group box 1 (HMGB-1), a highly conserved DNA binding protein, is known to be secreted by infection and interacts with TLR2 and TLR4, but HMGB-1 comes to play at a relatively late phase, 8–12 h after exposure to pathogens[1]. These data suggest that HMGB-1 is induced by TNF-α and IL-1β from immune cells that have been exposed to PAMPs. Moreover, in an animal model of sepsis, serum levels of HMGB-1 increased over the 18–72 h following infection and negatively affected survival[2]. Heat shock protein 70 (HSP70) has also been suggested as a putative endogenous ligand for TLR4 (ref. 3), but it is not yet known whether HSP70 secretion is associated only with infection.

Aminoacyl-tRNA synthetases (ARSs) are enzymes that ligate specific amino acids to cognate tRNAs for protein synthesis. Interestingly, human ARSs have acquired additional functions beyond their catalytic role in protein synthesis[4]. Human tryprophanyl tRNA synthetase (WRS) contains a unique N-terminal extension of 154 amino acids (aa) (N154). Within this peptide, a sequence homologous to the WHEP-TRS (a conserved helix-turn-helix domain in tryptophanyl (W), histidyl (H), glutamyl-prolyl (EP) and threonyl (T)-tRNA synthethase) is embedded from 8 to 64 aa (ref. 5). This unique N-terminal peptide can be truncated via alternative splicing or proteolytic cleavage, resulting in a 'mini-WRS' that lacks the N-terminal 47 aa (N47)[6]. The mini-WRS, but not FL-WRS, exhibits a potent angiostatic capability[7], implying that FL-WRS could work as a precursor for mini-WRS or as a ligand with distinct activity. Intriguingly, increased expression of WRS in clinical infections such as *Vibrio cholera*[8], human cytomegalovirus[9] and human hepatitis B virus[10] has been reported, suggesting a potential role of FL-WRS in immunological responses against pathogen infection. In this study, we investigated the secretion of FL-WRS in response to various pathogenic challenges and determined its function as an intrinsic defensive factor against infection.

Results

Increase of WRS serum levels in sepsis patients. To examine whether WRS secretion into blood correlates with infection, we

[1]College of Pharmacy, Seoul National University, Seoul 08826, Republic of Korea. [2]College of Korean Medicine, Daejeon University, Daejeon 34520, Republic of Korea. [3]Research Institute of Pharmaceutical Sciences, College of Pharmacy, Seoul National University, Seoul 08826, Republic of Korea. [4]Medicinal Bioconvergence Research Center, Seoul National University, Suwon 16229, Republic of Korea. [5]Graduate School of Nanoscience and Technology, Korea Advanced Institute of Science and Technology, Daejeon 34141, Republic of Korea. [6]Laboratory Animal Resource Center, Korea Research Institute of Bioscience and Biotechnology, University of Science and Technology, Daejeon 34113, Republic of Korea. [7]College of Veterinary Medicine, Chungnam National University, Daejeon 34134, Republic of Korea. [8]Department of Pharmaceutical Science, College of Pharmacy, Kyung Hee University, Seoul 02447, Republic of Korea. [9]Divison of Rheumatology, Department of Internal Medicine, Seoul St Mary's Hospital, The Catholic University of Korea, Seoul 06591, Republic of Korea. [10]The Rheumatism Research Center, Catholic Research Institute of Medical Science, The Catholic University of Korea, Seoul 06591, Republic of Korea. [11]Division of Allergy and Immunology, Department of Internal Medicine, Yonsei University College of Medicine, Seoul 03722, Republic of Korea. [12]Institute of Allergy, Yonsei University College of Medicine, Seoul 03722, Republic of Korea. [13]Departments of Bioinspired Science and Life Science, Ewha Womans University, Seoul 03760, Republic of Korea. [14]Korea Chemical Bank, Korea Research Institute of Chemical Technology, Daejeon 34114, Republic of Korea. [15]College of Pharmacy, Korea University, Sejong 30019, Republic of Korea. [16]Department of Pulmonary and Critical Care Medicine, Asan Medical Center, University of Ulsan College of Medicine, Seoul 05505, Republic of Korea. [†]These authors contributed equally to this work.
*e-mail: sungkim@snu.ac.kr; mirimj@dju.ac.kr

© 2016 Macmillan Publishers Limited, part of Springer Nature. All rights reserved.

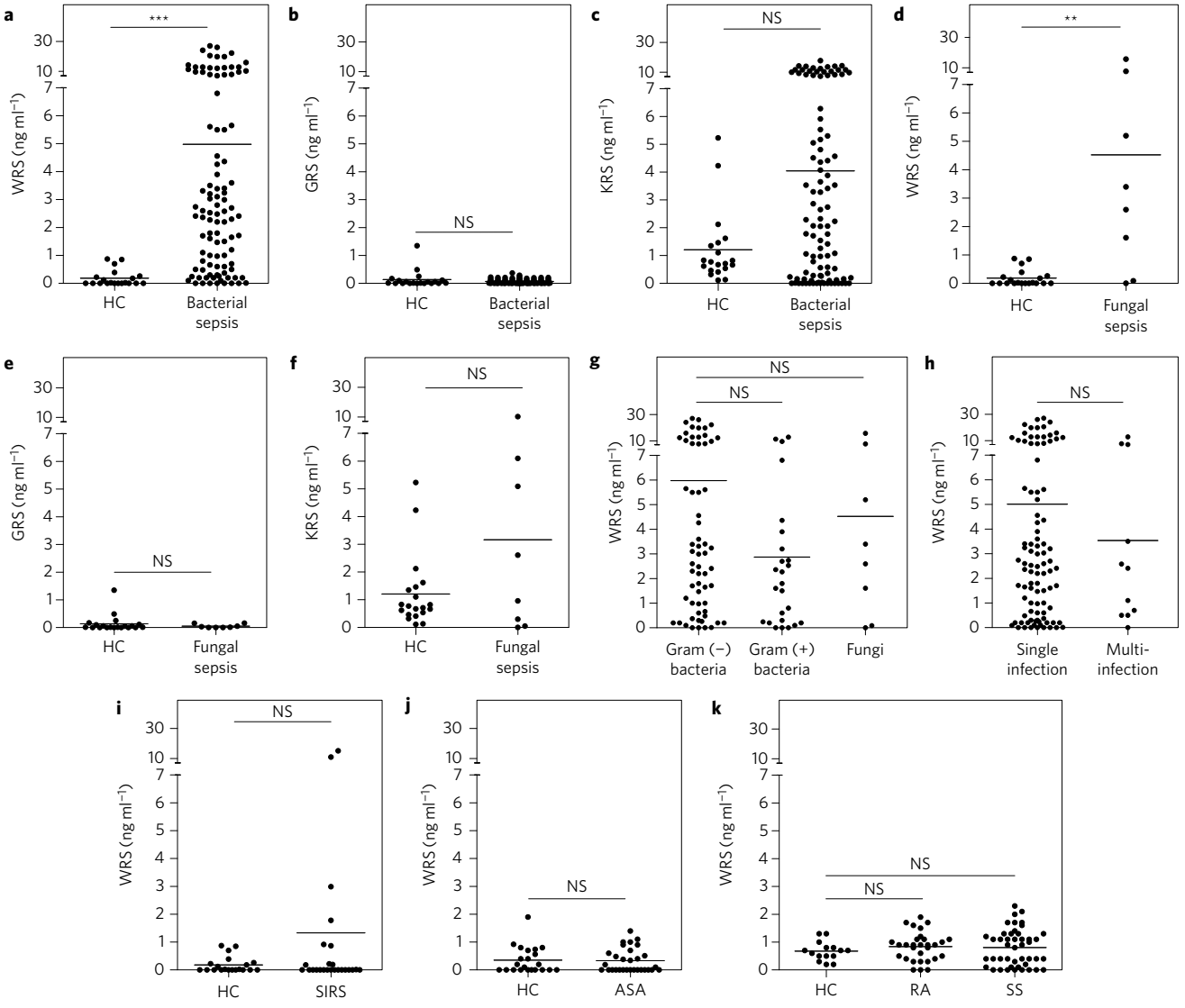

Figure 1 | Serum level of WRS in patients with sepsis and sterile inflammatory immune disorders. a–c, Serum levels of WRS (**a**), GRS (**b**) and KRS (**c**) in healthy controls ($n = 20$) and bacterial sepsis patients ($n = 100$) were measured by ELISA specific for each ARS. **d–f**, Serum levels of WRS (**d**), GRS (**e**) and KRS (**f**) in healthy controls ($n = 20$) and fungal sepsis patients ($n = 8$) were measured by ELISA. **g**,**h**, Comparison of serum levels of WRS in sepsis patients infected with Gram-negative bacteria ($n = 62$), Gram-positive bacteria ($n = 25$) and fungi ($n = 8$) (**g**) and with single ($n = 94$) or multiple ($n = 11$) pathogens (**h**). **i–k**, Serum level of WRS in healthy control ($n = 20$) and SIRS patients ($n = 25$) (**i**), in healthy control ($n = 22$) and ASA patients ($n = 30$) (**j**), and in healthy controls ($n = 15$), RA ($n = 30$) and SS ($n = 45$) patients (**k**) were measured by ELISA. Data are represented as scatter dots with means of triplicate measurements. HC, healthy control; NS, not significant, $^{**}P < 0.01$, $^{***}P < 0.001$, two-tailed Mann–Whitney test against healthy control.

measured serum levels of WRS in sepsis patients with systemic infection. Compared with healthy controls ($n = 20$, 0.18 ± 0.06 ng ml^{-1}), the levels of WRS increased about 27-fold in the sepsis patients with bacterial infection ($n = 100$, 5.0 ± 0.63 ng ml^{-1}, $P < 0.0001$) (Fig. 1a and Supplementary Table 1). In contrast, there were no differences in the levels of glycyl-tRNA synthetase (GRS) (Fig. 1b). Although lysyl-tRNA synthetase (KRS) appeared to show a higher mean value in sepsis patients than in healthy controls, the difference was statistically not as significant as the results for WRS (Fig. 1c) and additional analysis with more individuals seems to be necessary to reach a convincing conclusion. Levels of WRS, but not GRS and KRS, also increased in fungal sepsis patients ($n = 8$, 4.52 ± 1.83 ng ml^{-1}, $P < 0.01$) (Fig. 1d–f, and Supplementary Table 1). We did not observe significantly different levels of WRS among patients infected with Gram-negative bacteria ($n = 62$, 5.98 ± 0.93 ng ml^{-1}), Gram-positive bacteria ($n = 25$, 2.87 ± 0.72 ng ml^{-1}) and fungi ($n = 8$, 4.52 ± 1.83 ng ml^{-1}) (Fig. 1g), or between those with multiple ($n = 11$, 3.53 ± 1.22 ng ml^{-1}) and single ($n = 94$, 5.01 ± 0.67 ng ml^{-1}, $P > 0.05$) pathogen infection (Fig. 1h). To test whether WRS serum levels are increased in inflammatory immune disorders unrelated to infections, we measured WRS levels in sterile inflammatory disorders including systemic inflammatory response syndrome (SIRS), asthma patients (ASA), autoimmune disease patients diagnosed with rheumatoid arthritis (RA) and Sjogren's syndrome (SS) and found little difference between patients and healthy controls (Fig. 1i–k). These data suggest that systemic infection induces the secretion of WRS into blood.

Prompt secretion of WRS from monocytes following infection. To confirm that infection would induce the secretion of WRS, we measured the levels of WRS secreted from cultured human peripheral blood mononuclear cells (PBMCs) that were infected with various pathogens. Consistent with the data from sepsis patients, only WRS among the tested ARSs (including WRS,

© 2016 Macmillan Publishers Limited, part of Springer Nature. All rights reserved.

methionyl-tRNA synthetase (MRS), aspartyl-tRNA synthetase (DRS), GRS, histidyl-tRNA synthetase (HRS), KRS and ARS-interacting multi-functional protein 1 (AIMP1)) was detected in the culture medium (Fig. 2a). We observed increased secretion of WRS following infection of *Salmonella typhimurium* (ST), *Escherichia coli*, *Listeria monocytogenes*, *Staphylococcus aureus* and *Candida albicans*, up to 18-fold at 2 h after infection (Fig. 2b). At this time point, we did not observe significant secretion of HMGB-1 and HSP70. In addition, infection of respiratory syncytial virus (RSV) and PR8 influenza virus significantly induced WRS secretion (Supplementary Fig. 1a,b), indicating that WRS responds to diverse pathogenic infections.

After ST infection, the release of FL-WRS (and a low level of mini-WRS) into the medium was observed as early as 15 min, concomitant with a slight decrease in intracellular WRS levels (Fig. 2c and Supplementary Fig. 1c). In contrast, the intracellular precursor and mature secreted TNF-α were detected at 120 min after infection (Fig. 2c). HMGB-1, HSP70 and lactate dehydrogenase (LDH, a signature of cell death) were not observed during this period (Fig. 2c and Supplementary Fig. 1d). WRS mRNA levels were unchanged until 120 min after infection, whereas the TNF-α mRNA levels increased from 30 min until 120 min (Fig. 2d), suggesting pre-existing intracellular WRS was released immediately upon infection without *de novo* synthesis. WRS transcription was induced from 8 h after infection to restore normal intracellular WRS levels within 24 h (Supplementary Fig. 1e,f). In contrast, TNF-α mRNA synthesis reached its peak levels 2 h after infection and then decreased. Furthermore, intraperitoneal (i.p.) injection of ST also induced the secretion of WRS into the peritoneum within 1 h, and the level of mouse WRS secretion increased according to the amount of bacterial inoculum (Fig. 2e).

We then tested whether the WRS secretion is induced by pathogenic components or proinflammatory stimuli. Treatment of PBMCs with lipopolysaccharide (LPS), Pam3CSK4, CpG oligonucleotides (ODN) and zymosan induced WRS secretion in a dose-dependent manner. In contrast, other stimuli including TNF-α did not induce WRS secretion until 2 h (Fig. 2f). We asked whether endocytosis of pathogens is required for WRS secretion by monitoring the effect of endocytosis inhibitors such as dynasore and cytochalasin D, and found that the inhibitor-treated cells lost their WRS secretion activity (Fig. 2g,h). These results suggest that endocytosis of pathogen or pathogenic components, but not inflammatory stimuli, are required for WRS secretion. We then examined whether WRS was secreted from specific immune cells and found that only monocytes released significant amounts of WRS following infection (Fig. 2i). In summary, FL-WRS appears to be secreted from monocytes in response to the endocytosis of pathogens and this event occurs prior to the activation of innate immunity.

Effect of FL-WRS on innate immunity. To determine how FL-WRS functions in this rapid response to infection, we checked whether FL-WRS would affect phagocytic activities *in vivo* and *in vitro*. Phagocytic cells were captured and counted using *in vivo* imaging technology[11–13]. The number of phagocytic cells was significantly increased in the FL-WRS-treated mice compared to those in mini-WRS- and PBS-treated mice (Fig. 3a). Similarly, bone marrow-derived macrophages (BMDMs) treated with FL-WRS, but not mini-WRS, showed a significant increase in the uptake of *E. coli* particles (Fig. 3b).

Given that amplification of innate immunity depends on the productions of chemokines and the recruitment of inflammatory cells, particularly neutrophils and macrophages, we screened whether FL-WRS would induce chemokine and cytokine production in human PBMCs using a protein array (Supplementary Fig. 2a) and confirmed the positive effects of FL-WRS, but not mini-WRS, on the secretion and expression of TNF-α, MIP-1α and MIP-1β (Fig. 3c,d). These results are unlikely to be due to any residual LPS that might be present in FL-WRS, based on the following results. First, treating the cells with the LPS inhibitor polymyxin B did not reduce FL-WRS-induced chemokine production (Supplementary Fig. 2b). Second, performing a Limulus amebocyte lysate test revealed an endotoxin concentration of less than 0.05 EU μg^{-1}, which was not significant. Third, we prepared recombinant FL-WRS from HEK293T cells to avoid potential LPS contamination and observed that this protein also induced chemokine secretion (Supplementary Fig. 2c) to a level similar to that induced by *E. coil*-expressed FL-WRS. Consistent with the data from human PBMCs, i.p. injection of FL-WRS into the mouse peritoneum also increased the levels of TNF-α and MIP-1α (Supplementary Fig. 2d).

To evaluate the ability of FL-WRS to infiltrate immune cells, we conducted an *in vitro* transwell migration assay in which cell migration was detected towards the culture medium of FL-WRS-treated BMDMs and observed the migration of neutrophils and monocytes, but not B cells (Fig. 3e). Furthermore, *in vivo* time-lapse imaging experiments[11–13] showed that neutrophils and monocytes/macrophages were recruited to the injection site of FL-WRS, but not of mini-WRS (Fig. 3f). When mice were i.p. injected with FL-WRS, the numbers of $Ly6G^+$ neutrophils, $CD11b^+$ myeloid cells and $CD11b^+F4/80^+$ macrophages infiltrated into peritoneal exudate were increased fifteen-, nine- and twofold, respectively, compared with those injected with mini-WRS and the PBS-treated control (Fig. 3g).

To determine the cell types responding to FL-WRS, we treated various immune cells with FL-WRS and found that the secretions of TNF-α and MIP-1α were induced mainly from BMDMs (Fig. 3h). We also observed that FL-WRS induced cytokine production in human and murine macrophages (Supplementary Fig. 2e–g), reduced BrdU incorporation (Supplementary Fig. 2h) and increased the cell surface levels of macrophage activation markers such as CD40, CD80 and CD86 (Supplementary Fig. 2i). Furthermore, upon depletion of macrophages, FL-WRS-induced TNF-α and MIP-1α production in splenocytes (Fig. 3i) and the number of infiltrated neutrophils into the peritoneum were significantly reduced (Fig. 3j), indicating functional significance of macrophages in FL-WRS activity. All these results suggest that FL-WRS targets macrophages to activate innate immune responses.

***In vivo* effects of FL-WRS against infection.** We tested whether FL-WRS would protect mice from ST infection-induced lethality (Fig. 4a) using murine FL-WRS (mFL-WRS) and its N-terminal 51 aa deleted WRS (mΔN51-WRS) (Supplementary Fig. 3a). At 5 min after i.p. inoculation of ST, we injected mFL-WRS, mΔN51-WRS, or PBS into the mice and observed an increase in neutrophil infiltration (Fig. 4b) and decrease in the bacterial load in spleen and liver (Fig. 4c) that was also confirmed by histological examination (Fig. 4d) in mFL-WRS treated mice. In addition, 75% of the mFL-WRS-injected mice survived until 48 h after infection, whereas all of the PBS- and mΔN51-WRS-injected mice died within 48 h (Fig. 4e). Similar data were obtained for mice infected with *L. monocytogenes* (a Gram-positive bacterium) (Supplementary Fig. 3b–d), suggesting that treatment with FL-WRS in the early stage of bacterial infection could improve the survival rate.

To further validate the protective role of FL-WRS against infection, we prepared an antibody (scFv 4G1) that specifically binds to the N154 peptide of human WRS by panning a library of phage-displayed human single-chain variable fragments (scFv)[14] (Supplementary Fig. 4). Mice were i.p. injected with scFv 4G1 or scFv 2B (binding to human GRS) along with ST inoculation (Fig. 4f), and it was found that the scFv 4G1-treated mice showed a significant decrease in TNF-α and MIP-1α production (Fig. 4g), delayed neutrophil infiltration (Fig. 4h) and reduced mouse survival rate compared to the two other control groups (Fig. 4i). All of these results further validated the immunological importance of FL-WRS *in vivo*.

© 2016 Macmillan Publishers Limited, part of Springer Nature. All rights reserved.

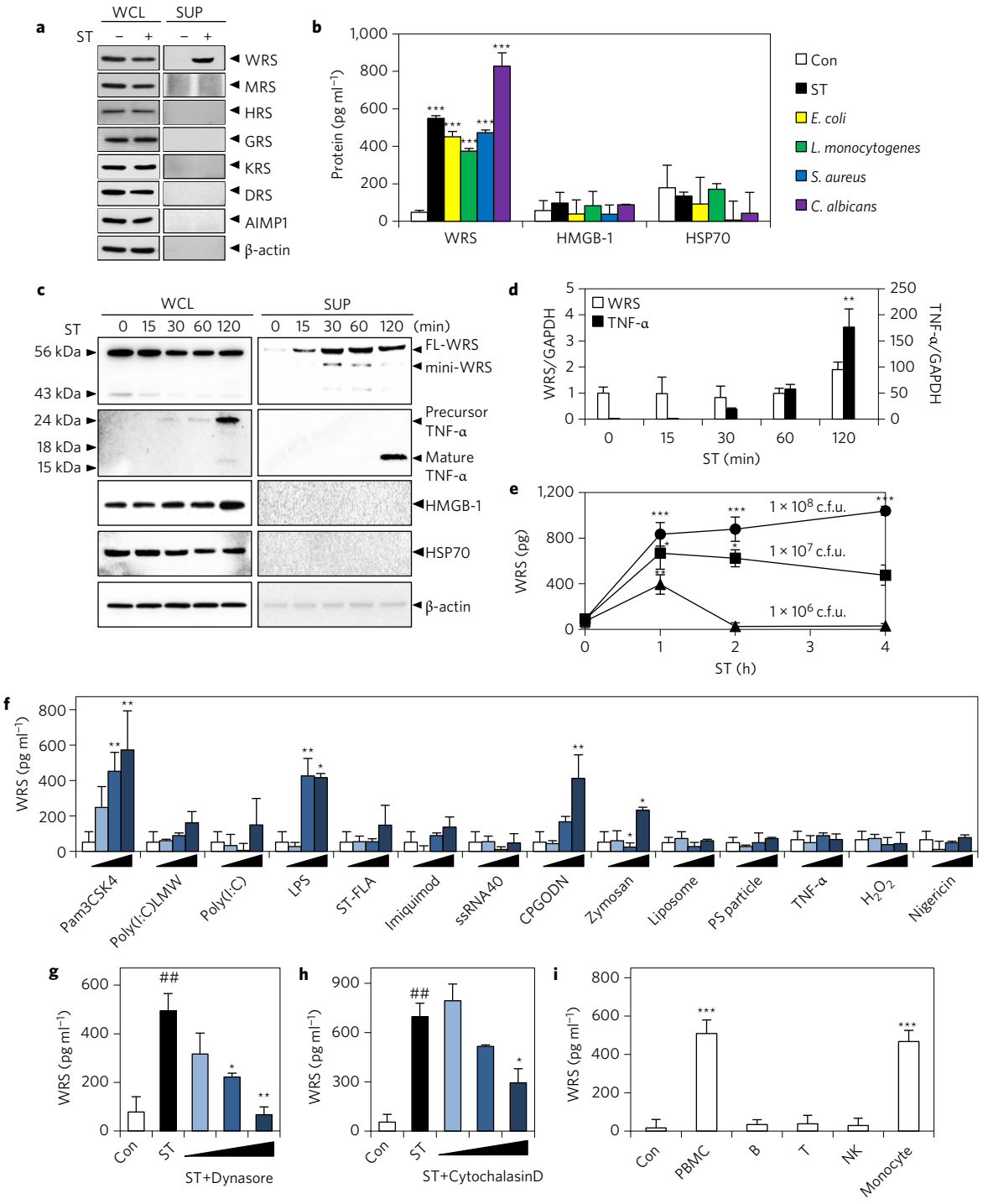

Figure 2 | WRS secretion from monocytes prior to TNF-α following infection. a, Levels of ARSs in the supernatants (SUP) and whole cell lysates (WCL) of *S. typhimurium* (ST)-infected human PBMCs (MOI = 1) for 2 h, detected by western blot analysis. **b**, Levels of WRS, HMGB-1 and HSP70 in culture supernatants of PBMCs following ST, *E. coli*, *L. monocytogenes*, *S. aureus* and *C. albicans* (MOI = 1) infection for 2 h, measured by ELISA. **c**, Levels of WRS, TNF-α, HMGB-1, HSP70 and β-actin in the SUP and WCL of ST-infected PBMCs (MOI = 1), detected by western blot analysis. **d**, mRNA levels of WRS and TNF-α in PBMCs infected with ST (MOI = 1) at the indicated time points, determined by real-time PCR. **e**, Mice were i.p. injected with the indicated c.f.u. of ST and the levels of WRS in peritoneal lavage were measured by ELISA. Data are shown as mean ± s.e.m. (n = 5–11 for each time point). c.f.u., colony forming unit. **f**, Level of WRS in the culture supernatants of PBMCs treated with increasing doses of Pam3CSK4, poly(I:C) LMW, poly(I:C), LPS (0.1–10 μg ml^{-1}), ST-FLA, imiquimod, ssRNA40, CPGODN (0.01–1 μg ml^{-1}), zymosan (0.1–10 μg ml^{-1}), liposome (0.005–0.5 mg ml^{-1}), polystyrene (PS) particles (1:1–10 cell-to-bead ratio), TNF-α (0.01–1 μg ml^{-1}), H_2O_2 (0.01–1 mM) and nigericin (10–250 μM) for 2 h, measured by ELISA. **g**,**h**, PBMCs were treated with dynasore (1–100 μM) (**g**) or cytochalasin D (1–100 μM) (**h**) for 30 min before ST infection, and the level of WRS in the cell culture supernatants was measured by ELISA. **i**, Subsets of immune cells were isolated from PBMCs and infected with ST (MOI = 1) for 2 h. The levels of WRS in the cell culture supernatant were measured by ELISA. In **b**,**d**,**f**–**i**, data are represented as mean ± s.d. of triplicate measurements. Statistical significance (*P < 0.05, **P < 0.01, ***P < 0.001) was determined against control (**b**,**d**,**f**,**i**) or ST-infected control, ##P < 0.01 compared with control (**g**,**h**) (one-way ANOVA). For **a** and **c**, experiments were repeated three times.

© 2016 Macmillan Publishers Limited, part of Springer Nature. All rights reserved.

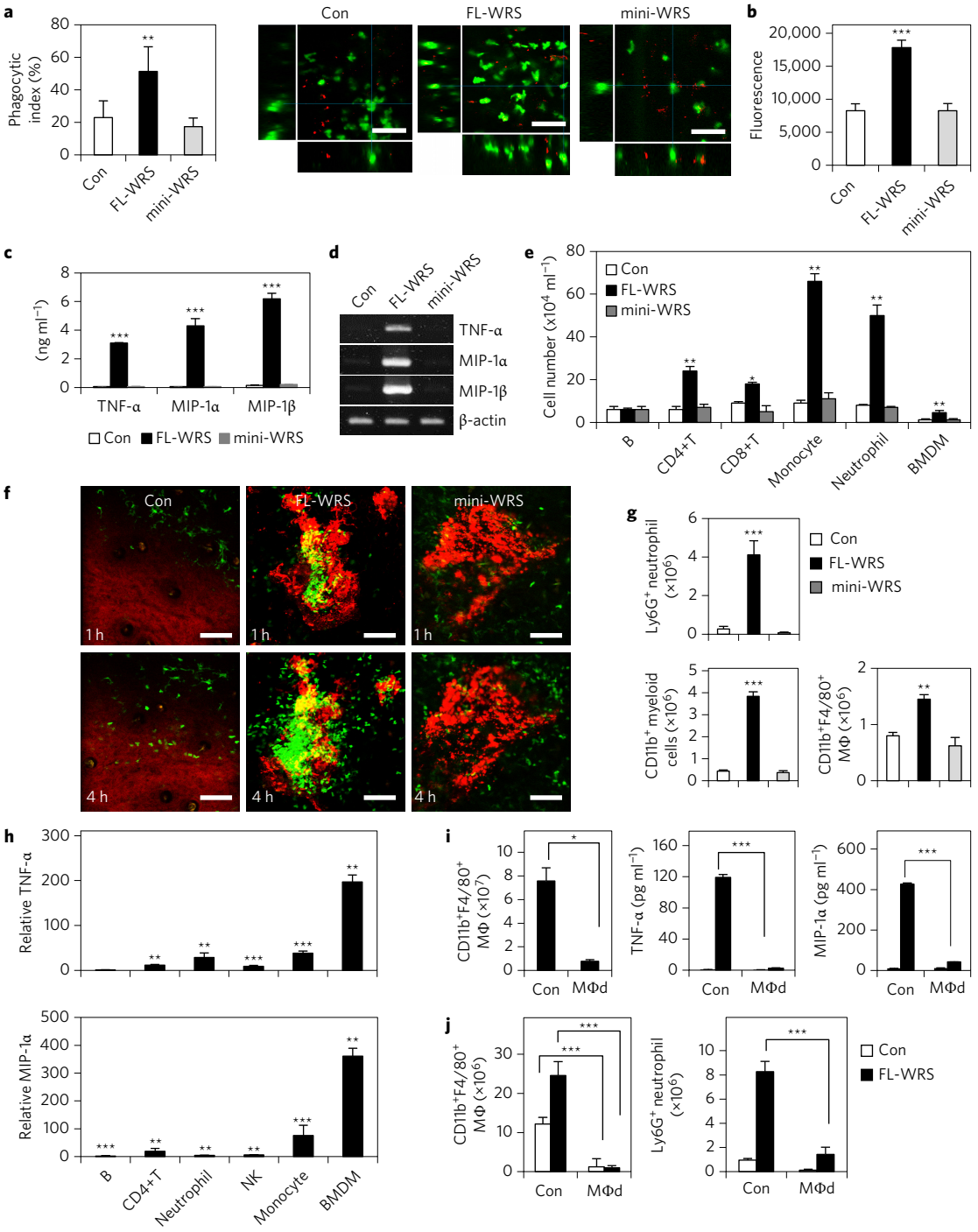

Figure 3 | FL-WRS, but not mini-WRS, activates macrophages to prime innate immune responses. a, Co-localization of Alexa647-labelled *S. typhimurium* (ST) and GFP-expressing cells was captured by an *in vivo* imaging system at 2 h following ST inoculation. **b**, BMDMs were treated with 100 nM FL-WRS and mini-WRS for 18 h and then incubated with FITC-labelled *E. coli* particles for 2 h. Phagocytosis of the particles was measured by a Vybrant phagocytosis assay kit. **c**,**d**, PBMCs were treated with PBS (Con), FL-WRS (10 nM) and mini-WRS (100 nM) for 3 h. Levels of TNF-α, MIP-1α and MIP-1β in the cell culture supernatants (**c**) and mRNA (**d**) were determined by ELISA and RT–PCR, respectively. **e**, Transwell migration assay. The number of primary immune cells migrated towards the culture supernatants of FL-WRS-treated BMDMs was counted. **f**, Infiltration of GFP-labelled cells by FL-WRS, mini-WRS (red fluorescence, each 0.1 μg) or PBS (Con), monitored by the *in vivo* imaging system. **g**, Mice were i.p. injected with PBS (Con), FL-WRS and mini-WRS (each 20 μg per mouse) for 4 h and the number of PECs was analysed by flow cytometry. **h**, Cultured mouse primary immune cells were treated with FL-WRS (100 nM) for 18 h and the levels of TNF-α and MIP-1α in the cell culture supernatants were measured by ELISA. The relative secretion was calculated by comparison with control. **i**, Splenocytes from macrophage-depleted mice (MΦd) were treated with FL-WRS (100 nM) for 18 h and the levels of TNF-α and MIP-1α were measured by ELISA. The number of $CD11b^+F4/80^+$ cells in splenocytes was analysed by flow cytometry. **j**, Macrophage-depleted mice were i.p. injected with FL-WRS (20 μg per mouse) for 4 h and the numbers of $CD11b^+F4/80^+$ and $Ly6G^+$ cells in PECs were analysed by flow cytometry. For **a**–**c**,**e**,**h**,**i**, data are shown as mean ± s.d. of triplicate measurements. For **g**,**j**, data are presented as mean ± s.e.m. ($n = 10$) of two independent experiments. Statistical significance (*$P < 0.05$, **$P < 0.01$, ***$P < 0.001$) was determined against control (one-way ANOVA). For **a**,**d**,**f**, experiments were repeated three times.

© 2016 Macmillan Publishers Limited, part of Springer Nature. All rights reserved.

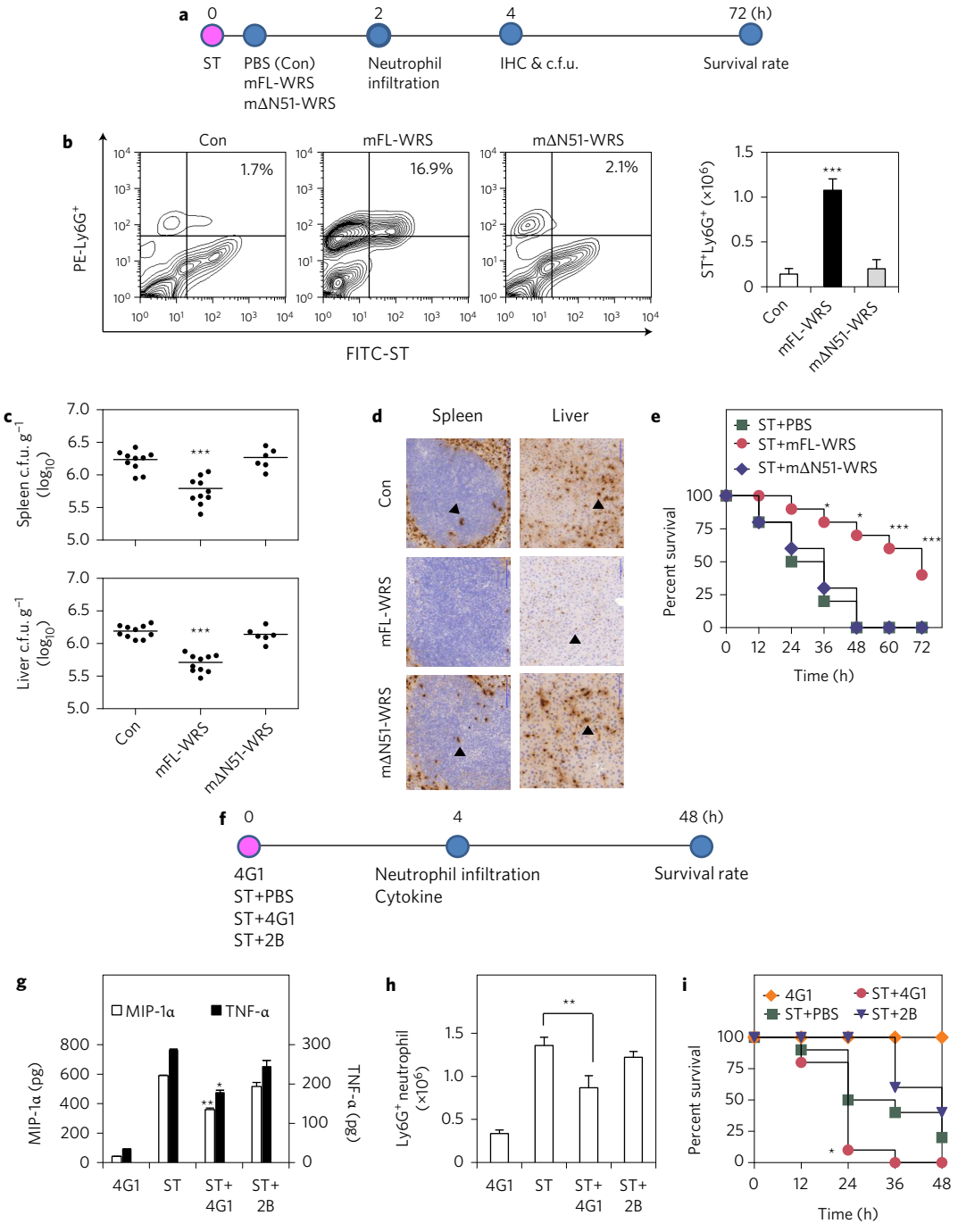

Figure 4 | FL-WRS protects bacteria-infected mice from lethality. a, Experimental scheme. Mice were i.p. injected with PBS (Con), mFL-WRS or mΔ51-WRS (each 20 μg per mouse) at 5 min after peritoneal *S. typhimurium* (ST) inoculation (1×10^7 c.f.u.). IHC, immunohistochemistry; c.f.u., colony forming unit. **b**, Mice ($n = 10$) were inoculated with FITC-labelled ST for 2 h and the percentage of peritoneal $Ly6G^+$ neutrophils (PE) was analysed by flow cytometry. **c**,**d**, Bacterial loads ($n = 6$–10) (**c**) and IHC (**d**) against ST in spleen and liver of mice at 4 h after ST inoculation. Arrows in **d** indicate ST. **e**, Survival rates of ST-infected mice ($n = 10$) treated with PBS (green), mFL-WRS (pink) and mΔN51-WRS (blue). **f**, Mice ($n = 10$) were i.p. injected with scFv 4G1 (anti-WRS, 100 μg per mouse) and scFv 2B (anti-GRS, 100 μg per mouse) followed by ST inoculation (1×10^7 c.f.u.). **g**,**h**, Levels of TNF-α and MIP-1α (**g**) and the number of PECs expressing $Ly6G^+$ (**h**) in peritoneal exudates were determined by ELISA and flow cytometry, respectively. **i**, Survival rates of ST-infected mice ($n = 10$) treated with PBS (green), scFv 4G1 (pink) or scFv 2B (blue). Uninfected mice ($n = 10$) treated with scFv 4G1 alone were used as negative control (orange). In **b**,**g**,**h**, data are presented as mean ± s.e.m. of two independent experiments. Statistical significance (*$P < 0.05$, **$P < 0.01$, ***$P < 0.001$) was determined against control (one-way ANOVA). For **c**,**e**,**i**, data are presented as means.

Identification of FL-WRS as an endogenous ligand of TLR2 and TLR4. To understand the molecular mechanism of FL-WRS, we applied FL-WRS to HEK293 cells expressing various PRRs and the NF-κB reporter system and found reporter induction in the cells expressing TLR4-myeloid differentiation factor 2 (MD2) and, to a lesser extent, TLR2 (Fig. 5a). TLR2 and TLR4 are surface-expressed PRRs that recognize microbial lipopeptides and LPS, respectively[15], and are involved in the activation of innate immune responses via NF-κB signalling[16]. We found that FL-WRS treatment induced nuclear translocation of NF-κB p65 and phosphorylation of IκB-α

© 2016 Macmillan Publishers Limited, part of Springer Nature. All rights reserved.

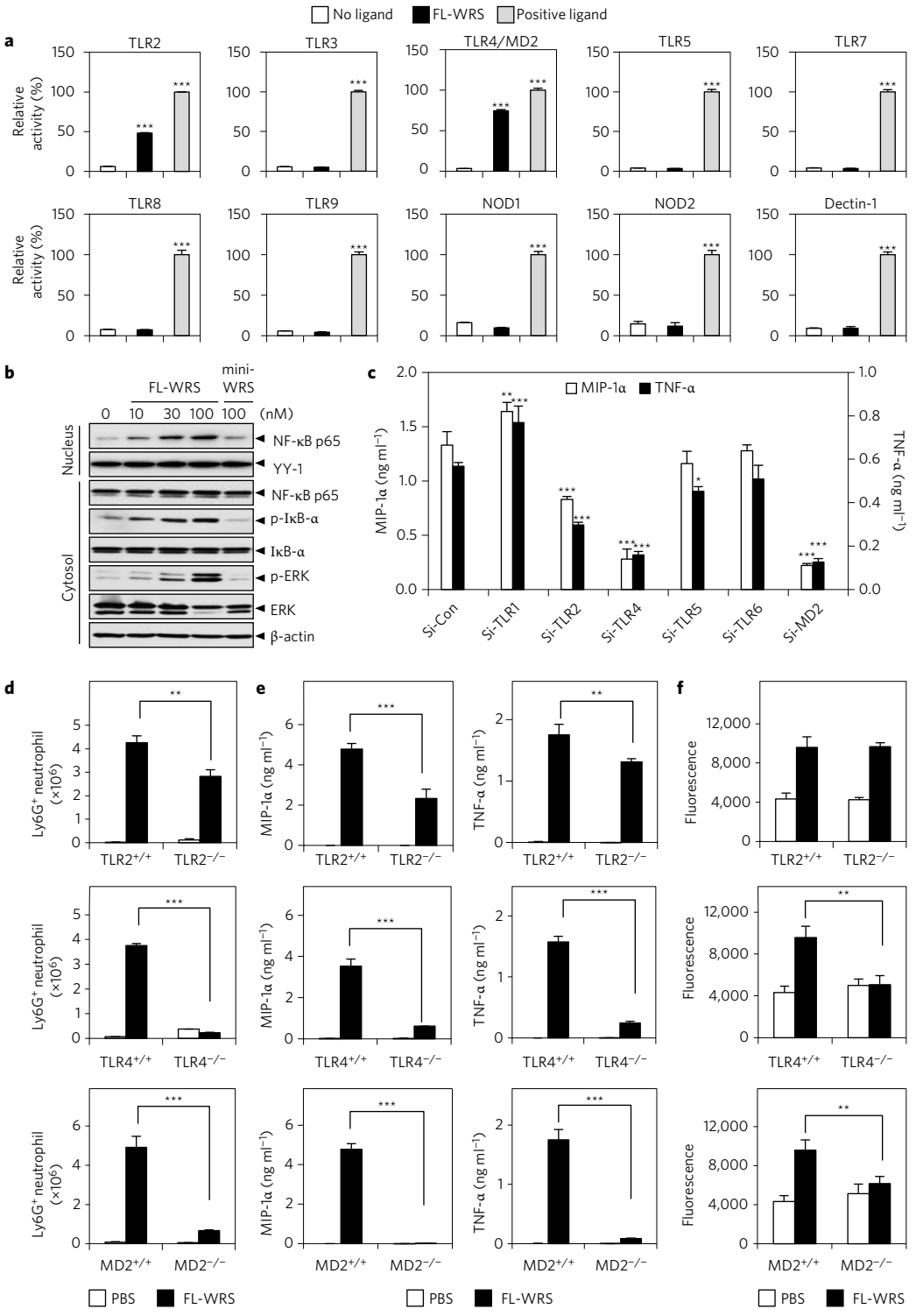

Figure 5 | Role of TLR4–MD2 and TLR2 in FL-WRS activation of innate immune responses. a, HEK293 cells expressing various PRRs and NF-κB SEAP reporter system were treated with FL-WRS (100 nM) for 18 h. The relative activity of alkaline phosphatase was calculated by comparing with that of cells treated with each positive control. **b**, Western blot analysis of nuclear and cytosolic fractions from J774A.1 cells treated with FL-WRS (10–100 nM) and mini-WRS (100 nM) for 30 min. YY-1 and β-actin were used as loading controls of nucleus and cytoplasm, respectively. **c**, TLRs were silenced in BMDMs using their respective siRNAs for 48 h followed by FL-WRS (100 nM) treatment for 18 h. Levels of TNF-α and MIP-1α in the culture supernatants were measured by ELISA. Scramble siRNA was used as a negative control. **d**, $TLR2^{-/-}$, $TLR4^{-/-}$, $MD2^{-/-}$, $TLR2^{+/+}$, $TLR4^{+/+}$ and $MD2^{+/+}$ mice ($n = 10$) were i.p. injected with FL-WRS (20 μg per mouse) or PBS for 4 h and the number of $Ly6G^+$ neutrophils in PECs was determined by flow cytometry. **e**,**f**, BMDMs prepared from bone marrow of $TLR2^{-/-}$, $TLR4^{-/-}$ and $MD2^{-/-}$ mice were treated with FL-WRS (100 nM) and PBS for 18 h. Levels of MIP-1α and TNF-α (**e**) in the cell culture supernatants and phagocytosis of FITC-labelled E. coli for 2 h (**f**) were determined by ELISA and Vybrant phagocytosis assay kit, respectively. In **a**,**c**,**f**, data are represented as mean ± s.d. of triplicate measurements. Statistical significance (*$P < 0.05$, **$P < 0.01$, ***$P < 0.001$) was determined against control (one-way ANOVA). In **d**,**e**, data are presented as mean ± s.e.m. of two independent experiments. Statistical significance (**$P < 0.01$, ***$P < 0.001$) was determined against $TLR2^{+/+}$, $TLR4^{+/+}$ and $MD2^{+/+}$ mice (one-way ANOVA). In **b**, experiments were repeated three times.

© 2016 Macmillan Publishers Limited, part of Springer Nature. All rights reserved.

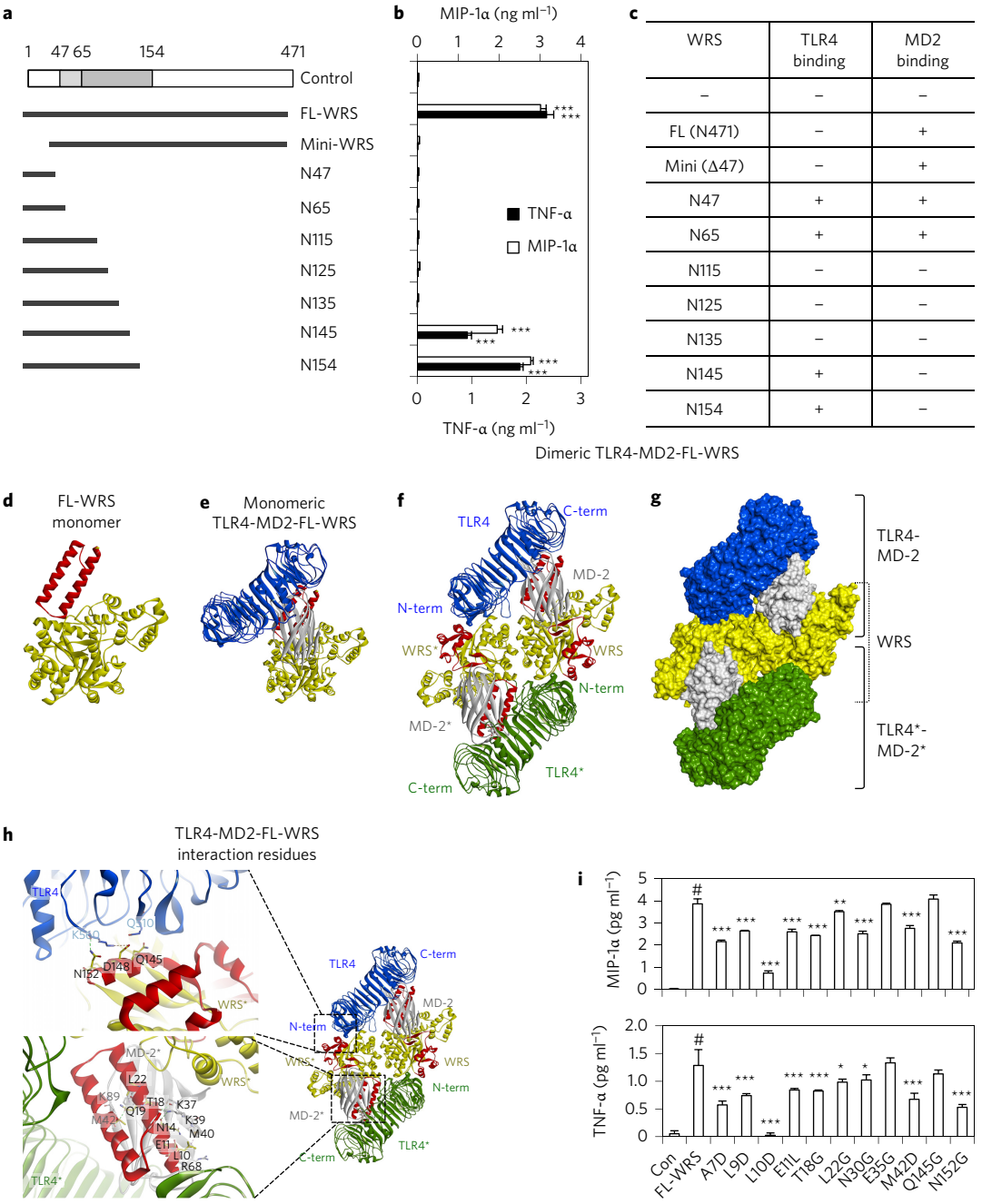

WRS	TLR4 binding	MD2 binding
–	–	–
FL (N471)	–	+
Mini (Δ47)	–	+
N47	+	+
N65	+	+
N115	–	–
N125	–	–
N135	–	–
N145	+	–
N154	+	–

Figure 6 | FL-WRS directly interacts with TLR4–MD2. a, Schematic diagram of FL-WRS, mini-WRS and a series of N-terminal peptides. **b**, Levels of TNF-α and MIP-1α were measured by ELISA in culture supernatants of BMDMs treated with FL-WRS, mini-WRS and a series of N-terminal peptides (100 nM each) for 18 h. **c**, Summary of SPR analysis for binding activities of N-terminal peptides with TLR4 or MD2. **d**–**g**, Putative binding model of TLR4–MD2 with the WRS homodimer based on a protein–protein docking study. **d**, Crystal structure of the FL-WRS (PDB code 1R6T) monomer. The structural information of the N1–6 and 61–81 aa peptides are missing. The helix-turn-helix WHEP domain spanning 8–64 aa is shown in red. **e**, Potential complex formation between TLR4–MD2 (blue and grey, respectively, PDB code 3FXI) and the WRS monomer (yellow). The peptide region spanning the WHEP domain (red) is predicted to interact with both TLR4 and MD2. **f**, Based on the model, TLR4–MD2 dimerization can be facilitated by bivalent interaction of the N154 peptides with two TLR4–MD2 units (blue and green) *in trans*. The two TLR4 interaction sites in N154 are shown (red) in a ribbon presentation. **g**, Complex structure of the 2:2:2 TLR4–MD2–WRS is represented in surface type. **h**, Highlighted putative regions and residues in N154 involved in the interaction with TLR4–MD2. **i**, Levels of TNF-α and MIP-1α in culture supernatants of BMDMs treated with WRS mutants (100 nM) for 18 h, measured by ELISA. In **b**,**i**, data are represented as mean ± s.d. of triplicate measurements. Statistical significance (*$P < 0.05$, **$P < 0.01$, ***$P < 0.001$) was determined against control (**b**) and FL-WRS, $^{\#}P < 0.01$ compared with control (**i**) (one-way ANOVA), respectively.

and extracellular signal-regulated kinases (ERK) in a dose-dependent manner (Fig. 5b).

To test whether the activity of FL-WRS would be affected by the knockdown of TLRs, we applied FL-WRS to BMDMs in which each of *TLR1*, *2*, *4*, *5*, *6* and *MD2* was silenced with their specific siRNAs. The results showed that the FL-WRS-induced TNF-α and MIP-1α production was significantly inhibited when TLR4, MD2 and TLR2 (to lesser degree) were suppressed (Fig. 5c). We also found that the FL-WRS-induced neutrophil infiltration was almost ablated in the TLR4$^{-/-}$ and MD2$^{-/-}$ mice, and partially reduced in

© 2016 Macmillan Publishers Limited, part of Springer Nature. All rights reserved.

TLR2$^{-/-}$ mice (Fig. 5d), and FL-WRS-dependent induction of cytokine production in all the knockout mice (Fig. 5e) and phagocytic activities in BMDMs were significantly suppressed in TLR4$^{-/-}$ and MD2$^{-/-}$ mice (Fig. 5f). Although i.p. injection of mFL-WRS after ST inoculation significantly diminished bacterial loads and improved survival rates in the TLR4$^{+/+}$ mice, these effects were not seen in TLR4$^{-/-}$ mice (Supplementary Fig. 5a,b). Together, these results suggest TLR4–MD2 (and possibly TLR2) to be a functional receptor for FL-WRS.

Proposed working mechanism of FL-WRS for TLR4–MD2 activation. To understand how FL-WRS would activate TLR4–MD2, we prepared a series of N-terminal peptides (Fig. 6a) and compared their cytokine production activities. Of these, N154 showed activity comparable to FL-WRS (Fig. 6b and Supplementary Fig. 6a) and its activity showed a dependency on TLR2, TLR4 and MD2 (Supplementary Fig. b), proving that N154 is sufficient to mediate the activity of FL-WRS.

The extracellular domain of TLR4 forms a stable heterodimer with MD2, and dimerization of the TLR4–MD2 complex occurs in the presence of LPS that is delivered to MD2 (ref. 17). We therefore tested whether FL-WRS would form a complex with TLR4 and MD2 in *in vitro* pulldown assays. Interestingly, both FL-WRS and mini-WRS were co-precipitated with TLR4 and MD2 (Supplementary Fig. 7a). In separate binding assays, both forms of WRSs bound to MD2 but not to TLR4 (Supplementary Fig. 7b,c), reminiscent of the binding mode of HMGB-1 to TLR4 through MD2 (ref. 18). Considering the results indicating that mini-WRS is completely inactive for cytokine production, the binding ability to TLR4–MD2 might not be the determinant for the ligand activity and that N47 (lacking in mini-WRS) would play a critical role for the activity although N47 itself cannot work as a fully active ligand.

Using surface plasmon resonance (SPR) analysis, we confirmed that FL-WRS and mini-WRS can bind to MD2 with a dissociation constant (K_d) of 190 and 200 nM, respectively (Supplementary Fig. 7d,e), but they showed no binding signal to TLR4 (Supplementary Fig. 7f,g). We also checked the binding of the different N-terminal fragments to MD2 and TLR4. Despite the fact that the N65-containing WHEP domain[5] and even its shorter fragment, N47, showed binding to both MD2 and TLR4, they did not induce cytokine production (Fig. 6b,c and Supplementary Fig. 7h,i,o,p), further suggesting that binding to TLR4 and MD2 is not sufficient for them to work as an active ligand. Interestingly, N115, N125 and N135 showed no binding to MD2 and TLR4 (Fig. 6c and Supplementary Fig. 7j–l,q–s, respectively) even though they contain the WHEP domain. Perhaps the peptide region beyond N65 can mask the WHEP domain from interaction with MD2. However, peptides longer than N135 (N154 and N145) partially restored the binding to TLR4, but not MD2 (Supplementary Fig. 7m,n), with cytokine-inducing activity (Fig. 6b,c and Supplementary Fig. 7t,u), suggesting that the peptide region beyond N135 might have an additional binding site for TLR4 and that this region would also be required for ligand activity.

Based on the data above and a previous modelling study of TLR4–MD2 dimerization by a homodimeric radioprotective 105 (RP105)/MD1 complex[19], we generated a binding model for the WRS homodimer[20] with two TLR4–MD2 complexes using their respective crystal structures. The docking model suggested that the N-terminal WHEP domain (8–64 aa) of the helix-turn-helix motif[20] (in red in Fig. 6d) would be inserted into the interface between TLR4 and MD2, leading to interactions with both proteins (Fig. 6e). This could explain why N47 is critical for the activity of FL-WRS. Furthermore, the model with two TLR4–MD2 complexes suggests an additional region spanning 145–152 aa (shown in red) that might interact with TLR4 *in trans* (Fig. 6f). Thus, N154 would be able to bring two TLR4–MD2 units for functional dimerization (Fig. 6f,g).

To validate this model, we introduced mutations at the residues that were proposed to interact with TLR4–MD2 (Fig. 6h and Supplementary Fig. 7v). Of these, the L10D mutation almost completely ablated the cytokine production activity (Fig. 6i), further confirming the functional importance of the N47 region. In addition, the N152G mutation also significantly reduced the cytokine-inducing activity, supporting the potential existence of the additional TLR4-binding site that would interact with TLR4–MD2 *in trans*. Taken together, N154 would be fully active as a ligand, facilitating the dimerization of the two TLR4–MD2 units (Supplementary Fig. 8). However, the isolated WHEP domain (N65) can only bind one unit of TLR4–MD2 because it lacks the secondary TLR4-binding site that is present in N154. Although mini-WRS lacking N47 can bring the two TLR4–MD2 complexes into proximity through homodimerization of the WRS catalytic domain[5], they may not be able to induce the functional dimerization of TLR4–MD2 to activate downstream signalling.

Discussion

This work provides evidence suggesting human FL-WRS as a novel endogenous ligand of TLR4, which promptly triggers innate immunity against infection. First, the secretion of FL-WRS would result from endocytosis of infectious agents (Fig. 2), rather than being indirectly triggered by pro-inflammatory stimuli. This is supported by the fact that WRS secretion into the blood is observed in patients with sepsis but not with SIRS or chronic autoimmune diseases (Fig. 1). In contrast, the extracellular release of HMGB-1 occurs not only as a result of infection[1], but also in response to various inflammatory disorders[21], and HSP70 is induced by SIRS, regardless of there being infection or not[22]. Second, FL-WRS responds promptly to pathogens before the onset of innate immune responses. Because FL-WRS is constitutively present in cells, it can be released immediately from monocytes, which are the first cells responding to infection, without the *de novo* synthesis that is usually required for the secretion of the known cytokines for innate immunity. Third, FL-WRS secretion can be induced by diverse pathogens (Fig. 2f and Supplementary Fig. 1), which could provide immunological flexibility. Fourth, FL-WRS appears to work primarily via TLR4 and possibly via TLR2. Through these receptors, FL-WRS could simultaneously sensitize strong and diverse immunological responses[23]. Fifth, FL-WRS primarily elicits its action against macrophages. As a result, FL-WRS may not only increase phagocytosis *in situ*, but may also clear pathogens by enhancing neutrophil infiltration via chemokines. With these features, FL-WRS appears to suppress the propagation of infected pathogens at an early stage while priming innate immune responses.

It is intriguing that both FL-WRS and mini-WRS could bind to TLR4–MD2, but mini-WRS is completely inactive in the induction of cytokines. Perhaps, the N-terminal 47 aa that are lacking in mini-WRS may be necessary for the correct orientation of the TLR4–MD2 dimers that is required for the activation of downstream signal pathways. In fact, N47 forms part of the WHEP domain in the structures of several different ARSs and it is implicated in the modulation of various protein–protein interactions and immune reactions[5]. The binding model and mutational analysis also explain why the peptides containing a partial or full WHEP domain of WRS (N47, N65) are not active, despite the fact that they could bind to both TLR4 and MD2. The bivalent ability of N154 interacting with two TLR4–MD2 complexes (via the WHEP domain and an additional site downstream) *in trans* appears to be necessary in order to work as the active ligand. It is not clear why the N154 peptide that is fully active as an immune stimulatory ligand was covalently attached to the catalytic domain of WRS during evolution. One possibility is that its expression and function

© 2016 Macmillan Publishers Limited, part of Springer Nature. All rights reserved.

can be secured by being attached to WRS, which is the indispensable enzyme for protein synthesis and cell viability. Another possibility is that the catalytic domain of WRS can also play an additional role in immunological responses against infection.

Although mini-WRS was inactive in terms of innate immunity, it is known to work as a potent anti-angiogenic ligand after secretion. In this case, in order to expose the active site cleft of WRS to the protruding tryptophan present in the extracellular domain of VE-cadherin, N47 needs to be removed[24]. Here, we report an active role of FL-WRS as an endogenous activator of TLR4. The anti-angiogenic activity of mini-WRS could serve as a feedback mechanism to prevent the chronic inflammation that may be caused by the sustained secretion of FL-WRS.

It is not clear at this moment whether FL-WRS should be considered a new component of innate immunity or as a distinct defensive mechanism that would prime innate immunity at an early stage of infection. Given that FL-WRS uses TLR4 (and possibly TLR2) as a functional receptor, it can be recognized as an extension of innate immunity. However, FL-WRS can be considered to be a unique defence factor recruited from protein synthesis machinery. It would be interesting to investigate whether the catalytic activity of WRS is involved in its extracellular activity. In any case, this work reports the functional connection of a protein synthesis enzyme to the host defence mechanism against infection. This finding also suggests that WRS can be used as an early biomarker and also as an immune stimulant against infection.

Methods

Human samples. Serum samples were collected from 20 healthy controls, 108 septic patients receiving intensive care for sepsis, and 25 SIRS patients without infection. All patients had been admitted to the intensive care unit of a university-affiliated hospital in the Republic of Korea, and only patients with proven bacterial and fungal infection were enrolled. The diagnosis of sepsis was based on the criteria presented at the ACCP/SCCM Consensus Conference in 1992 (ref. 25). This study was approved by the Institutional Review Board of the Asan Medical Hospital (2011–0001).

A total of 52 subjects who were admitted to the Severance Hospital Allergy-Asthma Clinics from January 2014 to July 2015 were enrolled. These subjects included 22 healthy control and 30 stable asthma patients who were diagnosed with asthma by allergy specialists, based on their symptoms and pulmonary function test results (>12% increase of forced expiratory volume for 1 s, FEV1) after bronchodilator use. This clinical study was approved by the Institutional Review Board, Severance Hospital and Yonsei University Health System (approval no. 4-2013-0397).

Sera were obtained from 45 patients with primary Sjogren's syndrome, 30 patients with rheumatoid arthritis (RA) and 15 healthy controls. Primary Sjogren's syndrome was diagnosed according to the American-European Consensus Group criteria for primary Sjogren's syndrome[26] or the 2012 American College of Rheumatology criteria[27]. RA was diagnosed according to 1987 revised criteria for the classification of RA[28] or the 2010 RA classification criteria[29]. This study was approved by the Institutional Review Board of Seoul St. Mary's Hospital (KC13ONMI0646). All human sera were obtained with informed consent.

Reagents and assay kits. Anti-TNF-α (catalogue no. 3707), anti-HMGB-1 (catalogue no. 3935), anti-HSP70 (catalogue no. 4872), anti-NF-κBp65 (catalogue no. 3034), anti-p-IκB-α (catalogue no. 9246), anti-p-ERK (catalogue no. 9101), anti-ERK (catalogue no. 9102) and anti-His-tag (catalogue no. 12689) were purchased from Cell Signaling Technology. Anti-CD11b-FITC (M1/70, catalogue no. 553310), anti-LY6G and Ly6C-PE (RB6-8C5, catalogue no. 553128), CD40-PE (3/23, catalogue no. 553791), CD80-PE (16-10A1, catalogue no. 553769) and CD86-FITC (GL1, catalogue no. 553691) were obtained from BD Pharmingen. Anti-F4/80-PE (BM8, eBioscience, catalogue no. 12-4801-80), TLR4 (R&D Systems, catalogue no. 1478-TR) and MD2 recombinant proteins (R&D Systems, catalogue no. 1787-MD) were also purchased. Anti-WRS (catalogue no. NMS-01-0009), anti-MRS (NMS-01-0003), anti-HRS (ref. 30), anti-GRS (NMS-01-0014), anti-KRS (NMS-02-0005), anti-DRS (NMS-01-0013) and anti-AIMP1 (NMS-01-0019) antibody were purchased from Neomics. A BrdU cell proliferation assay kit (Cell Signaling Technology, catalogue no. 6813), lactate dehydrogenase (LDH) cytotoxicity detection kit (Takara, catalogue no. MK401), Vybrant phagocytosis assay kit (catalogue no. V6694), ELISA kits for human WRS (Cusabio, catalogue no. CSB-E11789h), GRS (Cusabio, catalogue no. CSB-EL009262hu), KRS (MyBiosource, catalogue no. MBS067424), murine WRS (Cloud Clone Corp, catalogue no. SEB748mu), human HMGB-1 (Cloud Clone Corp, catalogue no. SEA399hu), human HSP70 (Cloud Clone Corp, catalogue no. SED506hu), human MIP-1α (R&D systems, catalogue no. DY270), human MIP-1β (R&D systems, catalogue no. DY271), human TNF-α (eBioscience, catalogue no. 88-7346-88), murine MIP-1α (R&D systems, catalogue no. DY150), murine MCP-1 (R&D systems, catalogue no. DY479) and murine TNF-α (eBioscience, catalogue no. 88-7324-88) were purchased as indicated. Each assay was performed according to the manufacturer's protocol. A human TLR1-9 Agonist Kit (Invivogen, catalogue no. tlr1-kit1hw), zymosan (Sigma, catalogue no. Z4250), human TNF-α (Peprotech, catalogue no. 300-01A), nigericin (Sigma, catalogue no. N7143), cytochalacin D (Sigma, catalogue no. C2618), dynasore (Sigma, catalogue no. D7693) and polystyrene latex beads (Sigma, LB30) were obtained as indicated. Dr H. Chun (Korea University, Republic of Korea) kindly provided liposome (200 nm size).

Bacteria, fungus and virus. *S. typhimurium* (ATCC 14028), *L. monocytogenes* (ATCC 15313), *E. coli*-K12 (ATCC 10798), *S. aureus* (ATCC 25923) and *C. albicans* (ATCC 10231) were obtained from the Korean Culture Center of Microorganisms. The numbers of overnight cultured bacteria and fungi were estimated from the absorbance at 600 nm using a predetermined calibration curve. Respiratory syncytia virus (RSV) A2 was propagated by inoculating with the human larynx carcinoma cell line, HEp-2 (CCL-23), as a monolayer with a previously prepared small-scale isolate stock (multiplicity of infection (MOI) = 0.01), and was collected when cytopathic effects were greater than 60%. Influenza A/Puerto Rico/8/1934 virus was propagated in specific pathogen-free embryonated eggs. Viruses were titrated by standard plaque assay.

Cell culture. Human PBMCs were isolated using a cell preparation tube with sodium citrate (Becton Dickinson, catalogue no. 362761). The human blood was obtained from healthy volunteers and the protocol was approved by the Institutional Review Board at Seoul National University (approval no. 1502/001-010). Human B cells (catalogue no. 130-101-638), T cells (catalogue no. 130-096-olp; 535), NK cells (catalogue no. 130-092-657) and monocytes (catalogue no.130-091-153) were prepared from human PBMCs using magnetic activated cell sorting (MACS, Miltenyi Biotec). Mouse B (catalogue no. 130-090-862) and T cells (catalogue no. 130-090-860) were prepared from mouse spleen. Mouse NK cells (catalogue no. 130-096-892), monocytes (catalogue no. 130-100-629) and neutrophils (catalogue no. 130-097-658) were prepared using MACS. BMDMs were differentiated from mouse bone marrow cells for 6–7 days with M-CSF (Peprotech, catalogue no. 315-02, 20 ng ml^{-1}). All isolated and cultured cells were determined by cell surface marker expression using FACS analysis.

HEK293T (human embryonic kidney 293T cell line, ATCC CRL-3216), THP-1 (human monocytic cell line, ATCC TIB-202) and J774A.1 (murine macrophage cell line, ATCC TIB-67) cells were purchased from American Type Culture Collection. The HEK293T and J774A.1 cells were grown in Dulbecco's modified Eagle's medium (DMEM) containing 10% fetal bovine serum (FBS) and 1% streptomycin and penicillin. THP-1 cell lines were grown in RPMI-1640 medium containing 10% fetal bovine serum (FBS), 1% streptomycin and penicillin, and 50 μM β-mercaptoethanol. Mycoplasma contamination was tested using a commercially available mycoplasma detection kit (Takara, catalogue no. 6601).

ELISA. The levels of WRS, GRS, KRS, HMGB-1, HSP70, TNF-α, MIP-1α, MIP-1β and MCP-1in the cell culture supernatants, peritoneal exudates lavage and human sera were determined using commercially available ELISA kits according to the manufacturer's protocol.

Western blot analysis. Cytosolic and nuclear extracts were prepared using a nuclear extract kit (Active Motif, catalogue no. 40010) and western blot analysis was performed according to previously described methods[31] using specific antibodies.

Recombinant protein purification. A series of human WRSs, N-terminal peptides, mutant WRSs, murine FL-WRS (mFL-WRS) and the N-terminal 51aa-deleted WRS (mΔN51-WRS) were cloned in pET-28a (His-tag) vector. WRS mutants were generated by site-directed mutagenesis kit (Agilent Technologies). The recombinant proteins were overexpressed in *E. coli* Rosetta2 (DE3) strain. The bacterial cells were lysed by sonication three times (10 s duration with 50 s interval). His-tagged proteins in supernatants were purified using a HiTrap HP column (GE Healthcare), followed by a HiLoad 16/600 Superdex 200 prep grade column (GE Healthcare Life Sciences). GST-tagged proteins were purified by glutathione-sepharose high-performance beads (GE Healthcare Life Sciences). Purified proteins were filtered using a Mustang E membrane (Pall Corporation). For preparation of the recombinant proteins from HEK293T cells, human *FL-WRS* and *mini-WRS* were cloned into pEXPR-IBA42 vector (IBA, catalogue no. 2-1942-000) designed for expression in cell culture supernatant. FL-WRS and mini-WRS were expressed in HEK293T cells for 48 h and purified from the cell culture supernatants using Ni-NTA resin (Invitrogen).

Reverse transcription-polymerase chain reaction (RT-PCR) and real time-PCR. RNA was extracted according to the protocol of the RNeasy kit (Qiagen, catalogue no. 74104) and the RNA samples were used for cDNA synthesis using a PrimeScript RT reagent kit (TaKaRa, catalogue no. PR037A). Quantitative RT-PCR was quantified using a 7500 real-time PCR system (Applied Biosystems) with Power SYBR Green PCR Master Mix (Applied Biosystems, catalogue no. 4367659). The mRNA levels of GAPDH and β-actin were used as internal controls. RT-PCR was

© 2016 Macmillan Publishers Limited, part of Springer Nature. All rights reserved.

performed according to previously described methods[31]. The gene-specific primer sequences are presented in Supplementary Table 2.

Cell migration assay. The cell migration assay was performed using a polycarbonate membrane transwell (Costar, catalogue no. 3421, 5.0 μm) coated with gelatin. Mouse primary cells were allowed to migrate for 4 h into the lower chamber and infiltrated cells were counted under a bright-field microscope.

Animal experiments. Animal experiments complied with the guidelines of the Daejeon University Animal Care and Use Committee (approval no. DJUARB2014-031). C57BL/6 mice (female, 9–10 weeks old) were purchased from Daehan Biolink Co.. Female LysM-GFP mice (lysozyme M-GFP, provided by Dr Kim at Rochester University) were used at ages between 12 and 17 weeks for *in vivo* imaging experiments. $MD2^{-/-}$ mice[32] were purchased from RIKEN BioResource Center (Ibaraki, Japan). C.-H. Lee and J.S. Lee provided the $TLR2^{-/-}$ and $TLR4^{-/-}$ mice[33,34]. The sample size (the number of mice per group) was chosen to enable statistical significance (generally more than five mice per group), and mice were randomly distributed into their respective groups. All experiments were conducted without blinding with age- and sex-matched mice. The counting of phagocytic cells in images obtained from *in vivo* imaging experiments was performed in a blinded manner. We included all the tested mice for analysis. The samples from each mouse were prepared in duplicate or triplicate for measurements and the experiments were repeated two or three times.

***In vivo* bacterial infection and bacteria counting.** *S. typhimurium* (ST) was grown to $OD_{600} = 0.5$ in nutrient broth (NB), washed in PBS at 10,000*g* and resuspended in PBS. ST was intraperitoneally infected with 1×10^7 colony forming units (c.f.u.) per mouse. After 4 h infection, spleen and liver were homogenized in 4 ml of distilled water (DW). The homogenized lysates were serially diluted to 1:10 with DW. The chosen dilutions (10 μl) were spotted four times on NB agar plates and incubated at 37 °C.

Preparation of WRS and GRS scFv. A phage-displayed human scFv library was panned against different recombinant human WRS as described previously[14]. Briefly, an immunotube was coated with 10 μg WRS and blocked with mPBS (PBS with 3% nonfat dried milk). The phage-displayed scFv library (1×10^{13} c.f.u.) in 1 ml mPBST (PBST with 3% nonfat dried milk) was added to the immunotube. After 2 h incubation, the tube was washed three to five times with PBST and the bound phages were eluted with 1 ml of 100 mM trimethylamine and neutralized with 0.5 ml of 1 M Tris-HCl (pH 7.0). ER2537 *E.coli* in mid-log phase was infected with the eluted phage and plated on LB-ampicillin plates supplemented with 2% glucose. On the following day, the bacteria were collected from the plates by adding 5 ml of LB medium to the plate and scraping off the bacteria with a glass spreader. Fifty microlitres of the collected bacteria were added to 20 ml SB (3% tryptone, 2% yeast extract, 1% MOPS, pH 7.0) plus ampicillin medium and grown for 2–3 h until $OD_{600} = 0.5$. VCSM13 helper phage (1×10^{11} plaque forming units, p.f.u.) was added and the infection continued for 1 h at 37 °C with slow shaking. Kanamycin (70 μg ml^{-1}) was subsequently added and the culture was incubated overnight at 30 °C with vigorous shaking. Next day, the culture was centrifuged and phage precipitation solution (4% PEG8000 and 3% NaCl, final concentration) was added and mixed thoroughly. After incubation on ice for 30 min, the precipitated phages were obtained by centrifugation and suspended in PBS and used for the subsequent round of panning. After four rounds of panning the library, individual scFv clones were screened by ELISA for their ability to bind WRS. The positive clones were sequenced to identify unique clones and each clone was expressed in *E. coli* and purified using a Ni-NTA affinity column. Anti-GRS scFv clone 2B was isolated from the same synthetic scFv library as scFv 4G1 using recombinant human GRS as an antigen. The clone specifically bound to GRS in immunoblot assays.

***In vivo* imaging system and image processing.** The Alexa647-labelled FL-WRS, mini-WRS (red fluorescence, each 0.1 μg) or PBS (Con) were injected intradermally into the ear of LysM-GFP transgenic mice. The infiltration of green fluorescence-labelled cells were monitored using an *in vivo* imaging system. Time-lapse imaging was performed with 30 s intervals at 1 or 4 h after injection (×20 magnification). For analysis of increased phagocytosis by FL-WRS, Alexa647-labelled ST (red) was co-injected with PBS, FL-WRS or mini-WRS into LysM-GFP transgenic mice ears. GFP-expressing cells that co-localized with red fluorescence were captured by the *in vivo* imaging system at 2 h following ST inoculation. The numbers of phagocytic cells were counted in five different fields and the percentage of phagocytic cells was calculated (>200 cells in each group). A custom-built video-rate laser-scanning confocal microscope imaging system modified from a previously designed system[11–13] was used to visualize immuno-cellular dynamics. Three continuous lasers with wavelengths of 488 nm (MLD, Cobolt), 561 nm (Jive, Cobolt) and 640 nm (MLD, Cobolt) were used as fluorescent excitation sources to achieve a three-colour fluorescent image. A fast-rotating 36-facet polygonal mirror (MC-5, aluminium-coated, Lincoln Laser) and galvanometer mirror (Cambridge Technology, 6230H) were used to obtain the two-dimensional scanning pattern. Emitted three-colour fluorescent signals from the intravital mouse model on a three-dimensional motorized *XYZ* translational stage (Sutter Instrument, MPC-200-ROE) were detected by high-sensitivity photomultiplier tubes (Hamamatsu, R9110) and digitalized by an eight-bit three-channel frame grabber (Matrox, Solios). A ×20 (Olympus, LUMFLN60XW, NA1.1) and a ×60 objective lens (Olympus, LUCPLFLN20X, NA0.45) generated 500 × 500 and 167 × 167 μm images of field views, respectively. Images were obtained with a Matrox Imaging Library (Matrox, MIL9) using custom-written imaging software with 512 × 512 pixels per frame at a frame rate of 30 Hz, and processed by Matlab (Mathworks) for *XY*-shift compensation and by ImageJ software (National Institutes of Health) for *XZ*/*YZ* axis reconstruction.

Flow cytometry. Cells were stained with antibodies for 30 min on ice in a binding buffer (PBS with 0.5% BSA and 0.01% NaN_3) and analysed by one- or two-colour flow cytometry on FACSCalibur (BD Biosciences) using FlowJo software (Flowjo LLC).

Immunohistochemistry. Paraffin-embedded sections were incubated in a solution of 0.3% H_2O_2 for 15 min to inhibit endogenous peroxidase activity. Sections were then incubated for 1 h at room temperature with primary antibodies (1:2,000 diluted) against *Salmonella* antibody (Novus Biologicals, catalogue no. NB600-1087). The detection system EnVision+ for rabbit antibodies (DAKO, catalogue no. K4003) was applied according to the manufacturer's instructions. Slides were stained with liquid diaminobenzidine tetrahydrochloride (DAB+), a high-sensitivity substrate–chromogen system (K3468, DAKO). Counterstaining was performed with Meyer's haematoxylin. The images on the slides were visualized with an Olympus Bx40 light microscope.

Macrophage depletion. To deplete macrophages in the spleen, mice were injected i.v. with liposomal clodronate (1 mg per mouse, Encapsula NanoSciences) for 24 h. To deplete macrophages in peritoneal exudate cells (PECs), mice were simultaneously injected both i.v. (0.5 mg per mouse) and i.p. (0.75 mg per mouse) with liposomal clodronate for 24 h. Control liposome was injected as a negative control of macrophage depletion.

PRR reporter assay. HEK293 cells expressing the SEAP reporter system (Invivogen) were treated with FL-WRS or each specific ligand (positive control) for mouse PRRs for 18 h (InvivoGen Study no. 157908). The ligands were HKLM (heat-killed *L. monocytogenes*, 1×10^8 cells per ml), poly(I:C) (1 μg ml^{-1}), *E. coli*-K12 LPS (100 ng ml^{-1}), *S. typhimurium* flagellin (ST-FLA, 100 ng ml^{-1}), CL097 (1 μg ml^{-1}), CL075 (10 μg ml^{-1}) + poly(dT) (10 μM), CpG ODN 1826 (100 ng ml^{-1}), C12-iEDAP (100 ng ml^{-1}), L18-MDP (100 ng ml^{-1}) and zymosan (hot alkali-treated *S. cerevisiae*, 10 μg ml^{-1}).

Si-RNA transfection. Mouse si-TLR1 (catalogue no. Tlr1-MSS211916), si-TLR2 (Tlr2-MSS216272), si-TLR4 (Tlr-MSS211922), si-TLR5 (Tlr5-MSS285031), si-TLR6 (Tlr6-MSS211925) and si-MD2 (Ly96-MSS275499) were purchased from Invitrogen. BMDMs (1×10^5) were plated in 48-well plates overnight and transfected with si-RNAs using X-tremeGENE siRNA Transfection Reagent (Roche Diagnostics, catalogue no. 04 476 093 001). Stealth universal RNAi (Invitrogen) was used as negative control.

***In vitro* pulldown assay.** FL-WRS and mini-WRS were cloned into pGEX4T-1 (GST-tag) vector. The recombinant proteins were overexpressed in *E. coli* Rosetta2 (DE3) strain. The bacterial cells were lysed by sonication three times (10 s duration with 50 s interval). GST-tagged WRSs were purified by glutathione-sepharose high-performance beads (GE Healthcare Life Sciences). Purified proteins were filtered using Mustang E membrane (Pall Corporation). GST, GST-FL-WRS or GST-mini-WRS (each 2 μg) in PBS were mixed with glutathione-sepharose beads at 4 °C for 2 h. Recombinant human TLR4 and/or MD2 (each 2 μg) proteins were added and the mixtures were incubated at 4 °C for 4 h. Proteins binding to beads were subjected to western blot analysis.

SPR. SPR experiments were performed using a Biacore T200 (GE Healthcare) equipped with a Series S sensor chip CM5 (GE Healthcare) at 25 °C. PBS buffer (KH_2PO_4 144 mg l^{-1}, NaCl 9,000 mg l^{-1}, Na_2HPO_4 795 mg l^{-1}, without calcium or magnesium) was used as a running buffer for the immobilization procedure. Immobilization was performed using an amine coupling kit (GE Healthcare). Flow cells were activated with a 7 min pulse of a 1:1 mixture of EDC (1-ethyl-3-(3-dimethylaminopropyl) carbodiimide hydrochloride) and NHS (N-hydroxysuccinimide) according to the manufacturer's recommendations. FL-WRS and mini-WRS were diluted with 10 mM sodium acetate (pH 5.0 for FL-WRS and pH 5.5 for mini-WRS) and immobilized to a Series S sensor chip CM5 to achieve immobilization levels of 600–1,600 and 600–1,500 response units (RU), respectively. In another set of experiments, human TLR4 and MD2 proteins were diluted with 10 mM sodium acetate (pH 5.0) and immobilized to the chip, giving a surface density of 1,000–2,600 and 600–1,000 RU, respectively. Flow cells were then blocked with a 7 min pulse of 1 M ethanolamine-HCl (pH 8.5). Serially diluted analytes or buffer were injected for 1–10 min at 30 μl min^{-1} flow rate and washed out for 20 min according to the analytes. Sensorgrams obtained with the reference channel were subtracted from those obtained with the channel with each protein.

© 2016 Macmillan Publishers Limited, part of Springer Nature. All rights reserved.

Protein–protein docking study. Interaction of WRS and TLR4-MD2 was simulated using ZDOCK and RDOCK in the Discovery Studio 4.5 software package (Biovia). The X-ray crystal structures of the human WRS (PDB code 1R6T) and TLR4-MD2 (PDB code 3FXI) were obtained from the Protein Data Bank (PDB). To assign the CHARMM force field for the protein–protein docking study, we modified the selenomethionine (Mse) residue of WRS to methionine (Met) using the Build Mutant protocol in Discovery Studio 4.5. We then generated a symmetric dimer of the WRS structure with chains including the N-terminal 7–60 aa of the X-ray crystal structure. The 13 docking models were chosen by high ZDOCK score and selection by eye from 2,000 proposed models. For further refinement by energy-based optimization, each pose was evaluated in RDOCK using the CHARMM polar H force field. We selected a final protein–protein docking model of 2:2 TLR4–MD2 dimerization bound to the WRS dimer using RDOCK energy and visual inspection.

Statistics. For all *in vitro* experiments, samples were tested in duplicate or triplicate and experiments were performed two or three times, independently. Data are shown as means ± standard deviations (s.d.) or as means ± standard error (s.e.m.). Statistical significance was calculated by one-way analysis of variance (ANOVA) following Tukey's test using SPSS software (version 21, IBM-SPSS). A two-tailed Mann–Whitney test was performed using GraphPad Prism version 5.01 (GraphPad Software). $P < 0.05$ was considered to be statistically significant.

Received 21 March 2016; accepted 2 September 2016; published 17 October 2016

References

1. Wang, H. *et al.* HMG-1 as a late mediator of endotoxin lethality in mice. *Science* **285,** 248–251 (1999).
2. Yang, H. *et al.* Reversing established sepsis with antagonists of endogenous high-mobility group box 1. *Proc. Natl Acad. Sci. USA* **101,** 296–301 (2004).
3. Vabulas, R. M. *et al.* HSP70 as endogenous stimulus of the Toll/interleukin-1 receptor signal pathway. *J. Biol. Chem.* **277,** 15107–15112 (2002).
4. Son, S. H., Park, M. C. & Kim, S. Extracellular activities of aminoacyl-tRNA synthetases: new mediators for cell–cell communication. *Top. Curr. Chem.* **344,** 145–166 (2014).
5. Guo, M., Yang, X. L. & Schimmel, P. New functions of aminoacyl-tRNA synthetases beyond translation. *Nat. Rev. Mol. Cell Biol.* **11,** 668–674 (2010).
6. Tolstrup, A. B., Bejder, A., Fleckner, J. & Justesen, J. Transcriptional regulation of the interferon-gamma-inducible tryptophanyl-tRNA synthetase includes alternative splicing. *J. Biol. Chem.* **270,** 397–403 (1995).
7. Wakasugi, K. *et al.* A human aminoacyl-tRNA synthetase as a regulator of angiogenesis. *Proc. Natl Acad. Sci. USA* **99,** 173–177 (2002).
8. Ellis, C. N. *et al.* Comparative proteomic analysis reveals activation of mucosal innate immune signaling pathways during cholera. *Infect. Immun.* **83,** 1089–1103 (2015).
9. Zhu, H., Cong, J. P., Mamtora, G., Gingeras, T. & Shenk, T. Cellular gene expression altered by human cytomegalovirus: global monitoring with oligonucleotide arrays. *Proc. Natl Acad. Sci. USA* **95,** 14470–14475 (1998).
10. Wieland, S., Thimme, R., Purcell, R. H. & Chisari, F. V. Genomic analysis of the host response to hepatitis B virus infection. *Proc. Natl Acad. Sci. USA* **101,** 6669–6674 (2004).
11. Choe, K., Hwang, Y., Seo, H. & Kim, P. *In vivo* high spatiotemporal resolution visualization of circulating T lymphocytes in high endothelial venules of lymph nodes. *J. Biomed. Opt.* **18,** 036005 (2013).
12. Faust, N., Varas, F., Kelly, L. M., Heck, S. & Graf, T. Insertion of enhanced green fluorescent protein into the lysozyme gene creates mice with green fluorescent granulocytes and macrophages. *Blood* **96,** 719–726 (2000).
13. Seo, H., Hwang, Y., Choe, K. & Kim, P. *In vivo* quantitation of injected circulating tumor cells from great saphenous vein based on video-rate confocal microscopy. *Biomed. Opt. Express* **6,** 2158–2167 (2015).
14. Yang, H. Y., Kang, K. J., Chung, J. E. & Shim, H. Construction of a large synthetic human scFv library with six diversified CDRs and high functional diversity. *Mol. Cells* **27,** 225–235 (2009).
15. Takeuchi, O. *et al.* Differential roles of TLR2 and TLR4 in recognition of Gram-negative and Gram-positive bacterial cell wall components. *Immunity* **11,** 443–451 (1999).
16. Fitzgerald, K. A. *et al.* Mal (MyD88-adapter-like) is required for Toll-like receptor-4 signal transduction. *Nature* **413,** 78–83 (2001).
17. Park, B. S. *et al.* The structural basis of lipopolysaccharide recognition by the TLR4–MD-2 complex. *Nature* **458,** 1191–1195 (2009).
18. Yang, H. *et al.* MD-2 is required for disulfide HMGB1-dependent TLR4 signaling. *J. Exp. Med.* **212,** 5–14 (2015).
19. Yoon, S. I., Hong, M. & Wilson, I. A. An unusual dimeric structure and assembly for TLR4 regulator RP105-MD-1. *Nat. Struct. Mol. Biol.* **18,** 1028–1035 (2011).
20. Yang, X. L. *et al.* Crystal structures that suggest late development of genetic code components for differentiating aromatic side chains. *Proc. Natl Acad. Sci. USA* **100,** 15376–15380 (2003).
21. Harris, H. E., Andersson, U. & Pisetsky, D. S. HMGB1 a multifunctional alarmin driving autoimmune and inflammatory disease. *Nat. Rev. Rheumatol.* **8,** 195–202 (2012).
22. Sonna, L. A. *et al.* Core temperature correlates with expression of selected stress and immunomodulatory genes in febrile patients with sepsis and noninfectious SIRS. *Cell Stress Chaperones* **15,** 55–66 (2010).
23. Sato, S. *et al.* Synergy and cross-tolerance between toll-like receptor (TLR) 2- and TLR4-mediated signaling pathways. *J. Immunol.* **165,** 7096–7101 (2000).
24. Zhou, Q. *et al.* Orthogonal use of a human tRNA synthetase active site to achieve multifunctionality. *Nat. Struct. Mol. Biol.* **17,** 57–61 (2010).
25. Bone, R. C. *et al.* Definitions for sepsis and organ failure and guidelines for the use of innovative therapies in sepsis. The ACCP/SCCM Consensus Conference Committee. American College of Chest Physicians/Society of Critical Care Medicine. *Chest* **101,** 1644–1655 (1992).
26. Vitali, C. *et al.* Classification criteria for Sjogren's syndrome: a revised version of the European criteria proposed by the American-European Consensus Group. *Ann. Rheum. Dis.* **61,** 554–558 (2002).
27. Shiboski, S. C. *et al.* American College of Rheumatology classification criteria for Sjogren's syndrome: a data-driven, expert consensus approach in the Sjogren's International Collaborative Clinical Alliance cohort. *Arthritis Care Res.* **64,** 475–487 (2012).
28. Arnett, F. C. *et al.* The American Rheumatism Association 1987 revised criteria for the classification of rheumatoid arthritis. *Arthritis Rheum.* **31,** 315–324 (1988).
29. Aletaha, D. *et al.* 2010 Rheumatoid Arthritis Classification Criteria: an American College of Rheumatology/European League Against Rheumatism collaborative initiative. *Ann. Rheum. Dis.* **69,** 1580–1588 (2010).
30. Park, S. G. *et al.* Human lysyl-tRNA synthetase is secreted to trigger proinflammatory response. *Proc. Natl Acad. Sci. USA* **102,** 6356–6361 (2005).
31. Park, S. *et al.* Pheophytin a and chlorophyll a suppress neuroinflammatory responses in lipopolysaccharide and interferon-γ-stimulated BV2 microglia. *Life Sci.* **103,** 59–67 (2014).
32. Nagai, Y. *et al.* Essential role of MD-2 in LPS responsiveness and TLR4 distribution. *Nat. Immunol.* **3,** 667–672 (2002).
33. Hoshino, K. *et al.* Cutting edge: Toll-like receptor 4 (TLR4)-deficient mice are hyporesponsive to lipopolysaccharide: evidence for TLR4 as the Lps gene product. *J. Immunol.* **162,** 3749–3752 (1999).
34. Takeuchi, O., Hoshino, K. & Akira, S. Cutting edge: TLR2-deficient and MyD88-deficient mice are highly susceptible to *Staphylococcus aureus* infection. *J. Immunol.* **165,** 5392–5396 (2000).

Acknowledgements

This work was supported by the Basic Science Research Program through the National Research Foundation of Korea (NRF) funded by the Ministry of Education (2010-0012505), Bio-Synergy/research Project (2014M3A9C4066465) and Global Frontier Project grants nos. NRF-M3A6A4-2010-0029785 and 2015M3A6A4065732 of the National Research Foundation funded by the Ministry of Science, ICT & Future Planning (MSIP) of Korea.

Author contributions

Co-first authors Y.H.A. and S.P. performed the experiments and analysed the data. J.J.C., B.-K.P., K.H.R., E.K., S.A., K.-S.I., N.H.K., H.S., B.W.H., P.K., J.-Y.L. and Y.J. performed experiments. C.-H.L. and J.S.L. provided knockout animals. M.-L.C., S.-H.P., K.P., H.J.P., J.H.L., J.W.P. and J.W.H. provided sera and discussed clinical data. M.J. and S.K. designed the experiments, supervised the research and wrote the paper. All authors approved the final manuscript.

Additional information

Supplementary information is available for this paper. Reprints and permissions information is available at www.nature.com/reprints. Correspondence and requests for materials should be addressed to M.J. and S.K.

Competing interests

The authors declare no competing financial interests.

© 2016 Macmillan Publishers Limited, part of Springer Nature. All rights reserved.